ACS APPLIED MATERIALS & INTERFACES

Research Article

www.acsami.org

Continuous Electrochemical Exfoliation of Micrometer-Sized Graphene Using Synergistic Ion Intercalations and Organic Solvents

Amr M. Abdelkader,*[,†,‡] Ian A. Kinloch,*[,‡] and Robert A. W. Dryfe[†]

[†]School of Chemistry, University of Manchester, Manchester M13 9PL, U.K.

[‡]School of Materials, University of Manchester, Manchester, M13 9PL, UK

Supporting Information

ABSTRACT: A novel top-down electrochemical method is demonstrated to prepare gram quantities of few-layer graphene in a single-step, one-pot process. Potential-controlled cathodic reduction is used to intercalate graphite electrodes with alkali-substituted, ammonium- and dimethyl sulfoxide-solvated cations. In situ decomposition of the intercalated compounds breaks the $\pi-\pi$ stacking of the graphene layers along the c axis of the graphite gallery, producing 1−20-μm-diameter few-layer graphene sheets, without the need for defect-inducing oxidative or sonication treatments. With a slight modification of the electrodes' configuration, the process can run in a continuous manner, presenting a potentially scalable approach for few-layer graphene production.

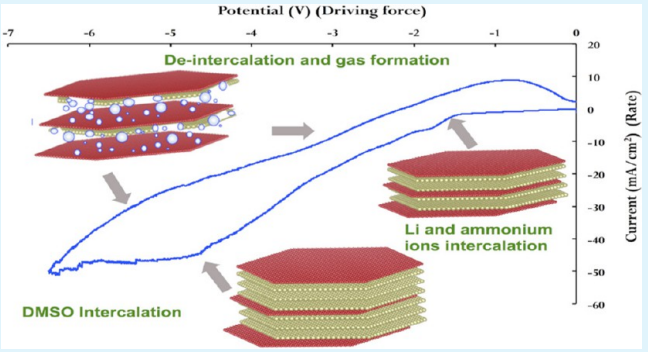

KEYWORDS: *graphene, electrochemical exfoliation, graphite-intercalated compounds, electrochemical functionalization*

1. INTRODUCTION

Graphene is a single-atom-thick, two-dimensional (2D) crystal consisting of sp^2-hybridized carbon atoms and exhibiting outstanding in-plane electrical properties and high mechanical strength.[1,2] The unique physical and chemical properties of graphene have attracted tremendous attention from both the academic and industrial communities since its isolation in 2004.[3,4] Currently, there are six main routes to produce graphene: mechanical exfoliation, chemical vapor deposition (CVD),[5,6] SiC thermal decomposition,[7] liquid-phase exfoliation,[8] and chemical and thermal reduction of graphene oxide (GO).[9−11] Mechanical exfoliation was the first method used to prepare graphene, and it is still used to prepare high-quality samples for research purposes.[12] However, this process is not suitable for scaling-up to the industrial level. CVD is capable of producing large sheets of graphene for electronic and display applications, but the process is not appropriate for producing graphene powder. Decomposition of SiC is expensive, and the product is mostly submicrometer in size, which limits its application.[7] The production routes for liquid-phase exfoliation and chemically reduced GO are simple processes and suitable for producing large quantities of graphene cheaply. However, such preparation methodologies need excessive toxic reducing agents and/or long-term sonication, which present some disadvantages in terms of scale-up. Moreover, some epoxide groups cannot be fully removed by chemical treatment and can degrade the electron mobility and other physical properties of the resultant reduced graphene.[9] Electrochemical methods, such as the recently developed electrochemical reduction of GO[13] or direct electrochemical exfoliation of graphite, are regarded as greener methods.[14] So far, the electrochemical approaches reported occur mostly at the anode and in electrolytes containing water. The produced graphene, or more correctly reduced graphite oxide, have a high density of sp^3 defects, and the produced materials are always contaminated by GO and other undesired carbonaceous species.[15,16] Recently, Loh et al. prepared graphene by electrochemical intercalation of Li^+ within the graphite galleries followed by dissociation of the resultant intercalating compound using prolonged sonication. Swager and Zhong tried to reduce the sonication time by intercalating graphite with lithium followed by a second intercalation of large organic ions.[17] In both cases, the strong decomposition reaction of the solvent cations hindered the formation of LiC_6 and/or ammonia−graphite intercalation compounds, and therefore full exfoliation was not achieved without the sonication step.[17] A further difficulty is that the carbonate solvents that have been previously used as electrolytes are subjected to nucleophilic attack at the carbonyl carbon and hydrogen abstraction at the *O*-alkyl carbon, which inevitably produces unwanted lithium carbonate (Li_2CO_3) and a variety of other lithium salts. These reactions lead to the poor intercalation of the lithium ions and the formation of carbon oxide gases on the surface of the electrode and not within the interlayer galleries.

In this work, graphite is fully exfoliated via an electrochemical process in organic solvents without the need of sonication or an

Received: October 15, 2013
Accepted: January 6, 2014
Published: January 6, 2014

   dx.doi.org/10.1021/am404497n | ACS Appl. Mater. Interfaces 2014, 6, 1632−1639

inert atmosphere. We also introduce a concept for the continuous production of graphene, which may be scaled-up. The electrolyte used was dimethyl sulfoxide (DMSO) containing lithium and small alkylammonium ions (triethylammonium, Et_3NH^+). DMSO was chosen as the organic solvent because it has a wide electrochemical window and its surface tension is close to the surface energy of graphite, preventing the detached graphene from restacking.[8] Lithium ions were able to intercalate before decomposition of the solvent. The exfoliation was enhanced further by the intercalation of Et_3NH^+ ions and the subsequent formation of triethylamine (Et_3N). The intercalation and decomposition of the solvent cations was found to play a critical role in the complete separation of the graphene layers. The produced material was predominantly few-layer graphene with particle sizes on the order of 1−20 μm. It is important to note that this material was produced without any sonication or centrifugation steps. Also, the process takes place at the cathode to avoid any oxidation of the graphite, potentially decreasing the density of the sp^3 defects.

2. ELECTROCHEMICAL EXFOLIATION

Figure 1a shows the cyclic voltammetry (CV) of graphite and platinum electrodes in DMSO and DMSO containing 1 M LiCl. While the CV of pure DMSO was featureless, it showed two reduction peaks before decomposition of the electrolyte when lithium ions were added. On the platinum wire, peaks were observed at −1.6 V. These may correspond to the underpotential deposition (UPD) of lithium on the electrode or to the reduction of some residual oxygen on the electrolyte.[18−20] The peak at −3.3 V (vs Ag/AgCl) is believed to correspond to the deposition of lithium. When graphite was used, the two reduction peaks were seen at −1.7 and −4 V (vs Ag/AgCl), respectively, and the current increased gradually between the two peaks. This prepeak current between the reduction waves is a well-known phenomenon because of the intercalation of Li^+ into graphite.[21] Further proof of lithium intercalating the graphite at low potentials was obtained by limiting the potential window to −2.5 V (Figure 1b). An oxidation peak was observed at −1.3 V for the graphite, showing delithiation, while the UPD peak on platinum had no corresponding oxidative response. The absence of the oxidative peak seems, for the first instance, to support the hypothesis that the peak at −1.6 V was for the reduction of residual oxygen. However, it has been reported that the UPD of lithium forming a thin layer on the surface of the noble metal and the detection of an oxidative peak depend on the scan rate. Moreover, as will be discussed later, lithium deposition takes place at a less negative potential on platinum than on the graphite electrode, which can be explained by the deposition of lithium on a lithium-containing film.

Examining the voltammetric response of DMSO saturated with Et_3NHCl on platinum and graphite electrodes (Figure 1c) can elucidate the role of the alkylammonium ions. It can be envisaged that the Et_3NH^+ ions lose a proton during the electrochemical reduction in a CE reaction (eq 1).[22,23] The reduction starts at −1 V (vs Ag/AgCl) on a platinum wire, and its oxidation couple in the reverse scan is in agreement with this hypothesis. On the graphite electrode, the reduction starts at a more negative potential with no oxidation in the narrow potential window, suggesting that the reduction process is not reversible on graphite. However, upon an increase in the potential limit to a more negative value (Figure 1d), the current increased gradually and a shallow reduction peak emerged at

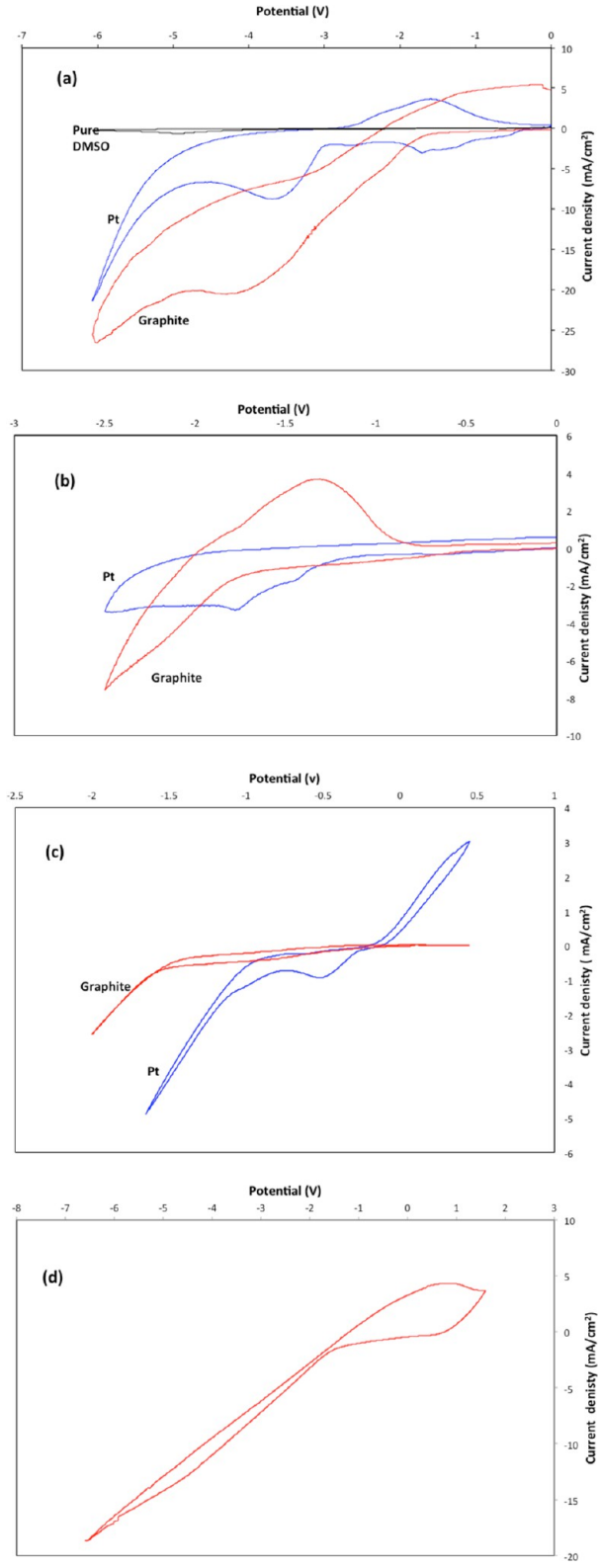

Figure 1. Cyclic voltammograms of platinum and/or graphite electrodes in a DMSO-based electrolyte: (a) with and without 1 M LiCl addition; (b) limited potential window for the 1 M LiCl electrolyte; (c) a Et_3NHCl-saturated solution; (d) wider potential window for a graphite electrode in a Et_3NHCl-saturated solution.

−4.7 V (vs Ag/AgCl) with a corresponding oxidation peak at 0.2 V. Black particles were observed coming out of the working electrode in the second cycle. It should be noted that the

dx.doi.org/10.1021/am404497n | ACS Appl. Mater. Interfaces 2014, 6, 1632−1639

electrode only eroded to form particles on the oxidation part of the cycle. The scanning electron microscopy (SEM) images of this powder showed a mixture of thin and expanded graphite (Figure S1 in the Supporting Information, SI), suggesting that the gradual increase in the current and shallow reduction peak at approximately −4.7 V is due to an intercalation process that leads to major expansion in the graphite crystal upon oxidation of the intercalated compound in the reverse scan. Because the oxidation peak, and the graphene/expanded graphite powder, was not observed when the CV was recorded on a graphite anode in an acetonitrile solution saturated with Et_3NHCl (Figure S2 in theSI) or with pure DMSO, it could be concluded that the process at high negative potential is a result of intercalation of a complex compound formed in two steps: the first step is the formation of solvated carbanion complexes through eqs 1−5,[24] and the second step is the formation of a DMSO−graphite intercalated complex compound[25] [the reaction of forming a DMSO−graphite intercalated compound and graphite intercalated with DMSO−Li−Et_3N complex(es) should be similar to eqs 1−5]. This intercalated compound could decompose cathodically if the potential is held at negative values according to reaction (6) or on the oxidation cycle according to reaction (7). In both cases, dissociation of the intercalated compound is associated with Et_3N gas formation, more likely taking place between the graphene layers, which pushes the graphene layers further apart.

$$2Et_3NH^+ + 2e^- = H_2 + 2Et_3N \quad (1)$$

$$nEt_3N + e^- + C = (Et_3N)_nC^- \quad (2)$$

$$Li^+ + e^- = Li \quad (3)$$

$$mLi + e^- + C = Li_mC^- \quad (4)$$

$$nEt_3N + mLi + e^- + C = Li_m(Et_3N)_nC^- \quad (5)$$

$$Li_m(Et_3N)_nC^- + e^- + 2Et_3NH^+ = C + mLi + (n + 2)Et_3N + H_2 \quad (6)$$

$$Li_m(Et_3N)_nC^- = C + mLi + nEt_3N + e^- \quad (7)$$

Figure 2a shows the CV of the graphite electrode when Li^+ and Et_3NH^+ were coexistent. The recorded voltammogram is a combination of the processes discussed for the separate ions. On a platinum electrode, there are three reduction peaks at −1.2, −1.9, and −3.2 V corresponding to the reduction of Et_3NH^+, the UPD of lithium, and the deposition of lithium. On graphite, the following phenomena were observed: (1) a reduction peak at −1.5 V corresponding to Et_3NH^+ reduction and formation of hydrogen, (2) a shallow reduction peak at −1.7 V followed by (3) a gradual decrease in the current associated with cointercalation of lithium and alkylammonium ions and (4) deposition of lithium, which is expected in this case to react with Et_3N from the previous step in a manner similar to the Birch reduction,[26,27] and (5) a current shoulder associated with the formation of a triethylamine−DMSO complex.

On the basis of these results, we fashioned an electrochemical program to apply a controlled cathodic potential on the graphite electrode, enabling the formation of exfoliated powder. The purpose of the customized electrochemical program is to (i) weaken the van der Waals interactions between the graphene sheets by intercalating the lithium and alkylammonium ions into the interlayer spacing, (ii) resemble the Birch reduction of graphite and reactions of a C_8MC_xM (where M is Li, Na, Ca, or K) graphite intercalated compound with weak protic acids in a tetrahydrofuran suspension,[28,29] (iii) allow the formation of a triethylamine−DMSO−graphite complex, and (iv) decompose a triethylamine−DMSO−graphite complex by oxidation. Therefore, a chronoamperometric step of −1.7 V versus Ag/AgCl was applied for 5 min followed by linear sweep voltammetry at a rate of 10 mV/s. The potential was then kept at −5 V for 5 min to allow intercalation of the electrolyte cations, and finally the potential was swept linearly back to the open-circuit potential to decompose the resultant complex compound.

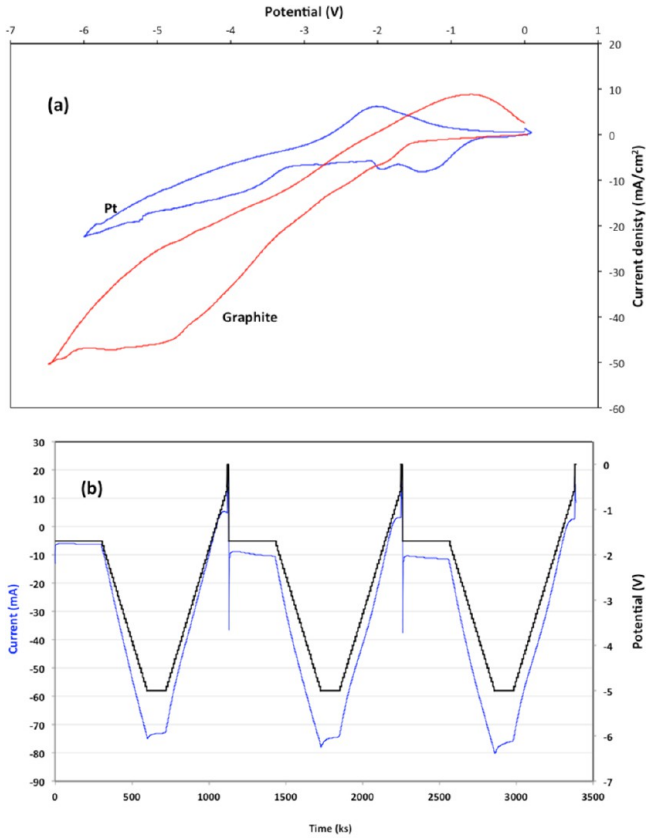

Figure 2. (a) Recorded CV of graphite (red) and platinum (blue) electrodes in DMSO with both LiCl and Et_3NHCl added to the electrolyte. (b) Optimized potential waveform used to synthesize graphene.

Figure 2b shows the programmed potential as well as the current response. Even before the end of the first cycle, a stream of very fine black powder was observed coming out of the graphite electrode. The progress of exfoliation of the graphite electrode is clear from the changing color of the electrolyte, as shown in Figure 2a (see the SI). The solid products were then collected by filtration and washed with water, dilute acid, and ethanol to remove any residue from the electrolyte. The powder was then dried overnight in a vacuum. Consumption of the electrolyte due to decomposition of DMSO was found to be minimal with only ∼0.9% volume decreased per hour of operation.

3. CHARACTERIZATION OF THE PRODUCED POWDER

The resulting black powder differed visually from the shiny metallic gray of the starting graphite. Various physical

dx.doi.org/10.1021/am404497n | ACS Appl. Mater. Interfaces 2014, 6, 1632−1639

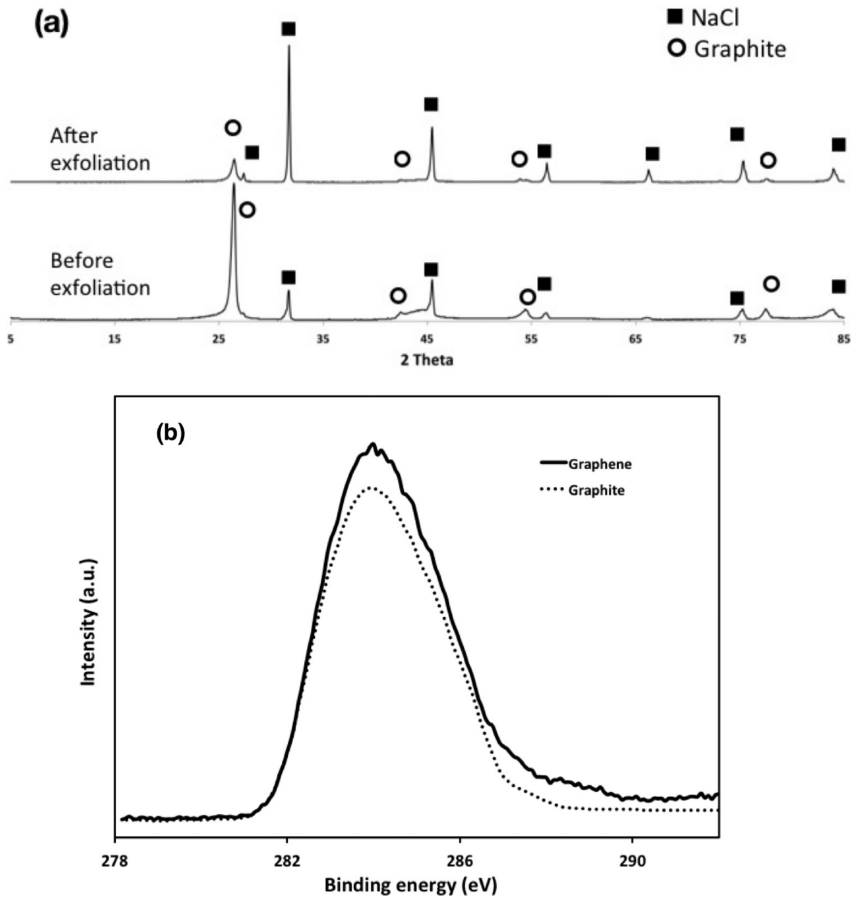

Figure 3. (a) XRD patterns for the produced solid. NaCl was added as a reference in a 1:1 weight ratio. Inset: (002) peak of graphite and the produced graphene. The X-ray source was Cu Kα. (b) High-resolution scans of the C 1s position for the produced graphene and the initial raw materials showing almost identical curves with slightly increased oxygen content for graphene.

characterization techniques were used to assess the product of the electrochemical process, and these clearly demonstrated that the product was predominantly few-layer graphene. The graphene flakes were first examined by X-ray diffraction (XRD) to assess whether the long-range periodicity associated with the *c* axis in bulk graphite had been modified. Figure 3a shows the XRD pattern of the produced powder mixed with NaCl reference in a ratio of 1:1 by weight. The (002) diffraction peak at around $2\theta = 26.6°$ from the interplanar repeat of the graphite has almost vanished upon exfoliation compared to the NaCl reference, indicating that the graphite layers have been separated. X-ray photoelectron spectroscopy (XPS) analysis found that the exfoliated powder had a low oxygen content, with only two peaks at 284.6 and 530.0 eV, corresponding to the C 1s and O 1s peaks, respectively. The high-resolution scans for the C 1s for the product and the initial graphite were almost identical, as can be seen in Figure 3b. The calculated oxygen content of the produced graphene was found to be 7.8 wt %, compared to 5.5 wt % of pure graphite, supporting the assumption about the largely nonoxidative nature of the process. The slight increase in the oxygen content can be attributed to an increase of the reactivity due to an increase of the surface area, including the creation of more terminated edge sites.

Raman spectroscopy has been accepted to be a very versatile technique for the characterization of graphene and to determine the number of layers. Parts a and b of Figures 4 show spectra and 2D peaks for representative examples of flakes with different numbers of layers recorded on an oxide-covered silicon substrate using a laser excitation of 633 nm. The G ($\sim$1580 cm^{-1}) and 2D ($\sim$2700 cm^{-1}) bands are clearly visible in all cases. It was possible to detect flakes with spectra that have an intense symmetric 2D band at 2650 cm^{-1} with full width at half-maximum = 65 cm^{-1}. These values are close to those reported in the literature for monolayer graphene.[30] However, analysis of the 2D band of 100 random graphene flakes showed that only 5% of the sample is monolayer. The histogram showed that flakes with all of the numbers of layers between 1 and 10 were produced (Figure 4c,d). The mean number of layers per flake is close to 5. It should be mentioned here that the Raman spectra were recorded by focusing the laser beam on the center of the flakes. The low percentage of graphite in the sample clearly showed a high degree of exfoliation.

Although the process does not involve any sonication step, which is believed to be the main source of defects in the graphene prepared by other chemical methods, the quality of the produced graphene was assessed using Raman spectroscopy. About 90% of the recorded Raman spectra have a D/G ratio of less than 0.5. This compares favorably with graphene powders synthesized by chemical approaches that show a strong D band in the Raman spectrum with an intensity ratio of D/G > 1. However, the D/G ratio of 0.5 probed with a red laser still corresponds to some defects in the graphene crystallites. Because the lateral dimension of the flakes is reasonably large (as will be discussed later), these defects

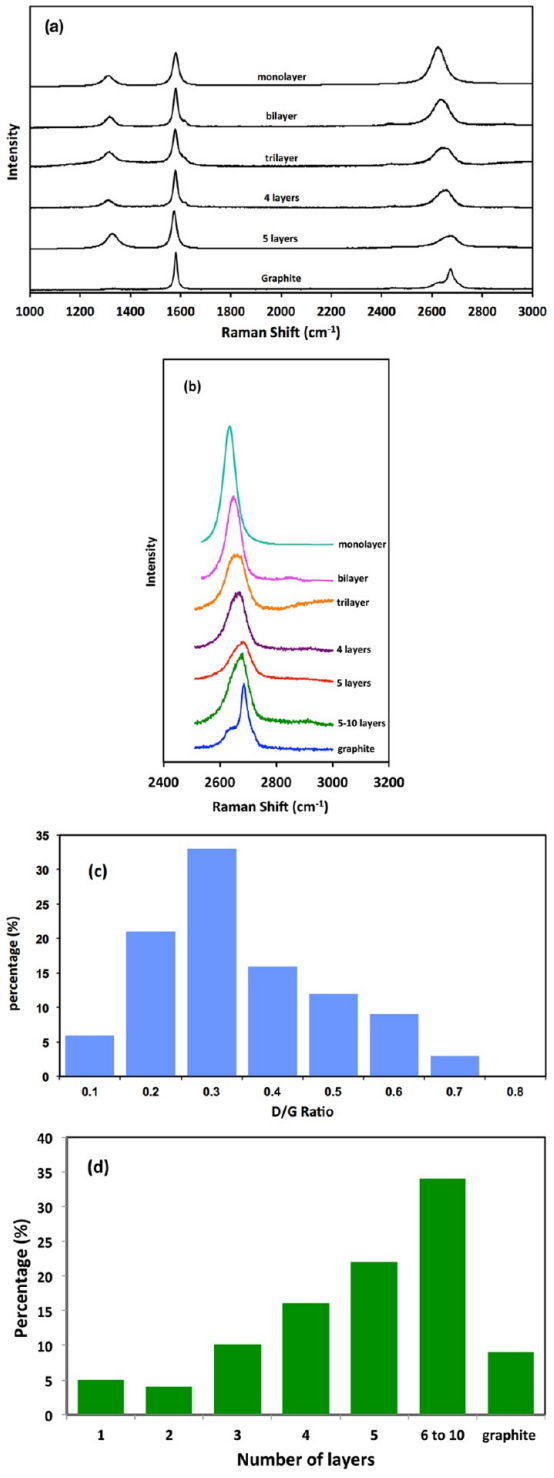

Figure 4. (a) Example of the Raman spectrum of exfoliated graphene on a silica substrate (excitation wavelength of 633 nm). (b) 2D band of the exfoliated graphene and the starting graphite materials showing that the electrochemical process produces different thicknesses of graphene flakes. (c) Histogram showing the relationship between the intensities of the D and G bands. (d) Histogram showing the number of layers per flake measured for 100 different flakes.

cannot be solely related to the edge effect. Also, XPS analysis (Figure 3b and the SI) showed a very low oxygen content on the surface of the graphene sheets, and therefore oxygen functional groups are not responsible for the emergence of the D band. Moreover, thermogravimetric analysis (TGA; see the SI) showed that the exfoliated materials decompose at a temperature lower than that of pristine graphite. If the sheets were completely intact, the energy to break the sp^2 C bond should be theoretically the same for graphene and graphite. All of these results suggested that there are some defects on graphene perhaps introduced by gas evolution between the layers or by fatigue caused by repeated intercalation/deintercalation.

Atomic force microscopy (AFM) has also been used to characterize the solid obtained. Statistical analysis of the thickness of the graphene sheet ensemble showed that all of the graphene sheets had thicknesses lower than 5 nm, with about 5% of the sheets lower than 0.9 nm. These statistics are in good agreement with Raman observations. Figure 5 shows a representative example of the exfoliated graphene (more examples of the AFM measurements can be found in the SI). The lateral size of these graphene sheets ranged from 1 to 15 μm, which is significantly larger than that produced by chemical or liquid-phase processes with prolonged sonication.

The size and morphology of the graphene sheets were further investigated by SEM and transmission electron microscopy (TEM). For that purpose, a diluted graphene solution was prepared by sonicating the exfoliated powder in chloroform for 30 min followed by dropping the solution on a silicon wafer substrate for SEM imaging and on a copper grid for TEM analysis. In both cases, the samples were dried under vacuum for 12 h at 100 °C. Figure 6a shows examples of the SEM images of the resultant graphene sheets, in which the size of the sheet ranged from 1 to 20 μm (see also the SI). The small flakes on the silicon substrate showed flat morphology with well-defined, sometimes folded, edges and sharp corners. However, the larger flakes had highly wrinkled morphologies. The flakes were thin enough to appear transparent under the SEM beam (see Figure S7 in the SI). The wide-range image showed aggregation and clustering of the flakes. The small flakes tend to stack flat and form layered clusters of 5−10 sheets, which are rarely observed by SEM imaging. The more predominant type of cluster was a mixture of small and large flakes, forming a more curly morphology. It is worth noting that the SEM images did not suffer from the charging problems associated with nonconductive groups on the surface of the GO sheets. The TEM images also confirm aggregation of the flakes (see the SI), with high-resolution TEM (HRTEM) of the flake edges revealing the well-defined layer structure of the multilayer graphene (the inset of Figure 6b). The electron diffraction (inset of Figure 5c) has a typical 6-fold symmetry, confirming that the graphene sheet is of a high-quality crystalline nature.

A conceptual cell design for a continuous process is illustrated in Figure 7. In this design, a consumable graphite cathode is inserted at the bottom of the cell. The reference electrode, as well as the anode (either lithium, platinum, or carbon), was inserted from the top. Exfoliation takes place at the cathode, and the resulting graphene sheets leave the cathode and are suspended in the electrolyte. The non-exfoliated, partially exfoliated, and expanded graphite that leave the cathode fall down to the bottom part of the cell by gravity, where they again contact the cathode for further exfoliation. The cathode is moving slowly, and a fresh part of the graphite rod cathode is entering the cell at a constant speed. The electrolyte is supplied via a special inlet near the cathode so that some of the graphene suspension leaves the cell from the outlet located at the top. A laboratory-scale version of the conceptual

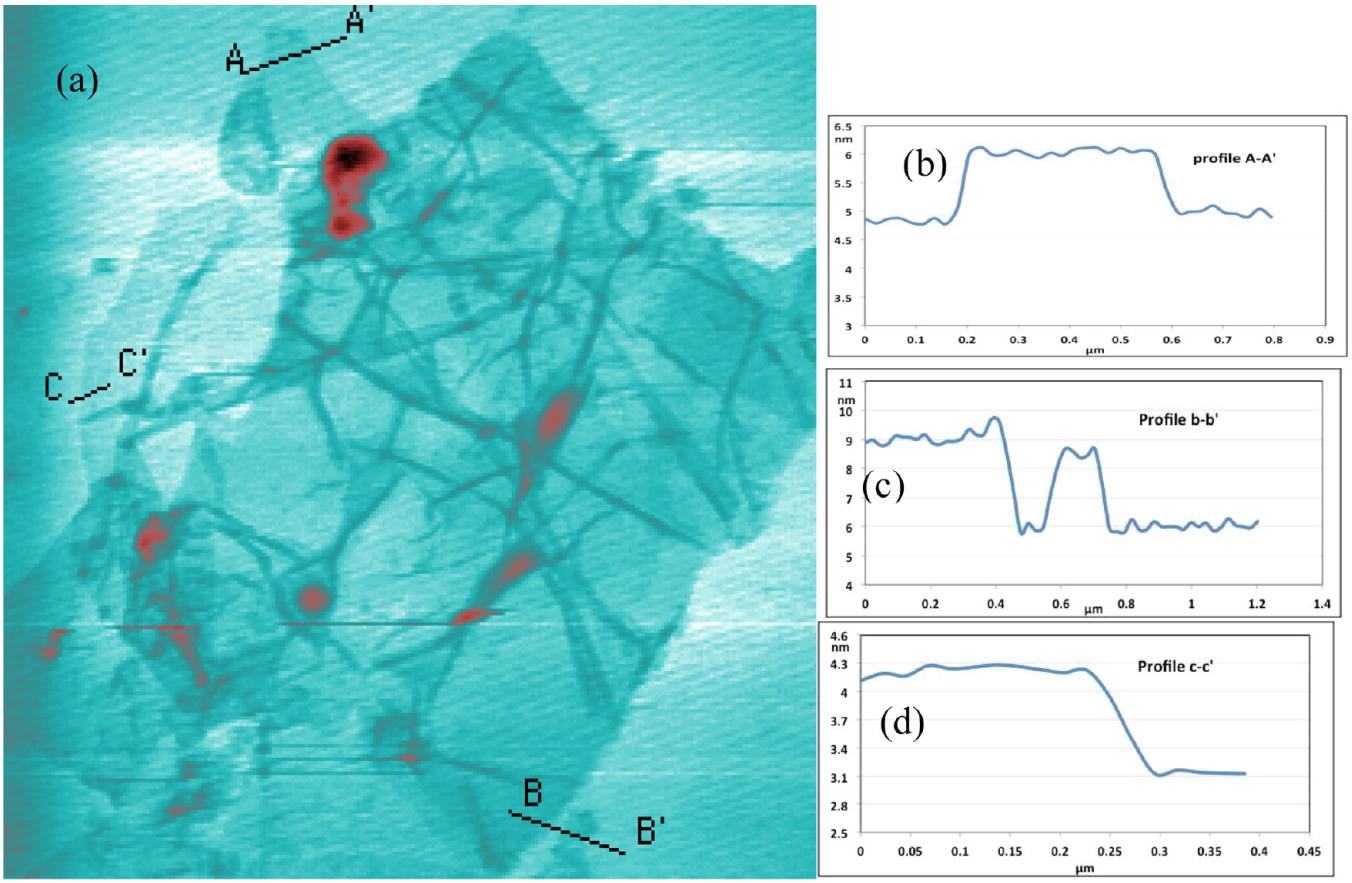

Figure 5. AFM measurement of the produced graphene sample, demonstrating high exfoliation of the original graphite after electrochemical exfoliation. (a) Tapping-mode image and (b–d) AFM section analysis, indicating the thicknesses of different flakes where the black lines A–A′, B–B′, and C–C′, respectively, cross several sheets.

cell design was tested in our lab for continuous production of 0.5–2 g of few-layer graphene per hour. The product was similar to that obtained by the batch process. Further details on the characterization of the graphene flakes produced by a continuous approach can be found in the SI.

4. CONCLUSIONS

In summary, we have developed an electrochemical technique for the high yield preparation of graphene sheets at the cathode to avoid oxidation of the product. The possible mechanism of the exfoliation process has been discussed. The particle size of the product predominantly ranges between 1 and 20 μm, and the thickness ranges from monolayer to several-layer graphene. The proposed method is tunable and can also be used to prepare functionalized graphene and graphene composites. We have also demonstrated the possibility of running the process in a continuous manner, increasing the productivity of the method.

5. EXPERIMENTAL SECTION

Electrochemical Exfoliation. Graphite and poly(vinylidene fluoride) (5 wt %) were mixed together in ethanol using a magnetic stirrer. The slurry was then dried overnight in a vacuum oven, the dry powder was pressed into 12-mm-diameter pellets or rods and sintered at 450 °C under argon, and then the resulting porous pellet was inserted as a working electrode. Platinum mesh was used as a counter electrode and Ag/AgCl as a reference electrode. The liquid electrolyte was prepared by dissolving lithium chloride (Sigma Aldrich, 99.9%) and/or triethylamine hydrochloride in dimethyl sulfoxide (DMSO; Sigma Aldrich, 99.9%). The cyclic voltammogram and customized potential-controlled program were conducted using an IviumStat potentiostat (Ivium Technologies, Eindhoven, The Netherlands). The exfoliation products were washed with water and ethanol until the pH was neutral, and the products were separated by filtration using Anodisc alumina membranes with 100 nm pore size and then dried at 200 °C under an argon atmosphere. In some cases, the resultant powder was pressed into pellet form and the exfoliation process was repeated to achieve full exfoliation.

Characterization of the Produced Powder. Raman spectra were obtained using a Renishaw system 1000 spectrometer coupled to a helium–neon laser. The laser spot size was ~1–2 μm, and the power was about 1 mW when the laser was focused on the sample using an Olympus BH-1 microscope. AFM images were obtained using a Multimode Nanoscope V scanning probe microscopy system (Veeco, Plainview, NY) with *Picoscan v5.3.3* software. Tapping mode was used to obtain the images under ambient conditions. The morphologies of the graphite and GO were also observed by SEM using a Carl Zeiss SUPRA SMT AG scanning electron microscope (LEO1525, Carl Zeiss, Oberkochen, Germany) with an accelerating voltage at 5 kV. TEM analysis used a FEI Tecnai F20 microscope. The samples were supported on a 3 nm ultrathin carbon-film-supported copper TEM grid (G3347N, Agar Scientific). Samples for XRD were prepared by mixing graphite powder or exfoliated powder with NaCl as a reference material. XRD analysis was conducted using a Philips X'PERT APD powder X-ray diffractometer (λ = 1.54 Å, Cu Kα radiation). TGA was performed in air using a Jupiter Netzsch STA 449 C instrument. The sample was placed into an alumina crucible and heated at a rate of 10 °C/min from 30 °C up to 800 °C.

dx.doi.org/10.1021/am404497n | *ACS Appl. Mater. Interfaces* 2014, 6, 1632–1639

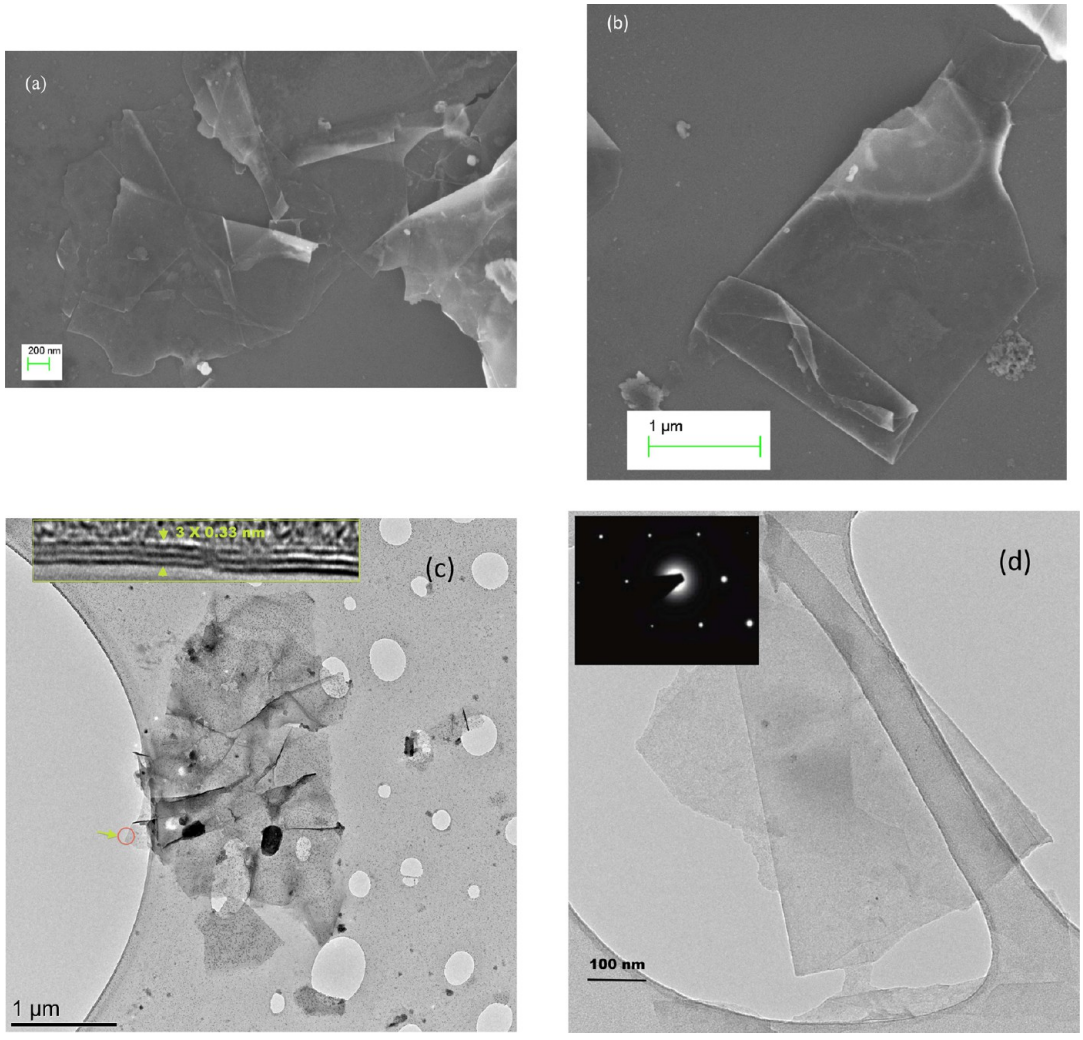

Figure 6. (a) SEM image for the sample showing as-synthesized graphene sheets agglomeration. (b) SEM image for an individual graphene sheet showing sharp edges and folding on the edges indicating a high degree of exfoliation. (c) TEM image of the produced graphene. Inset: HRTEM image of the edge of the graphene sheet showing a three-layer sheet. (d) TEM images of graphene. Inset: electron diffraction pattern showing a bilayer graphene. Analysis of the diffraction intensity ratio $I(0{-}110)/I(1{-}210)$ gives a value of 0.44, revealing that the flake is more likely to be a bilayer graphene.[31]

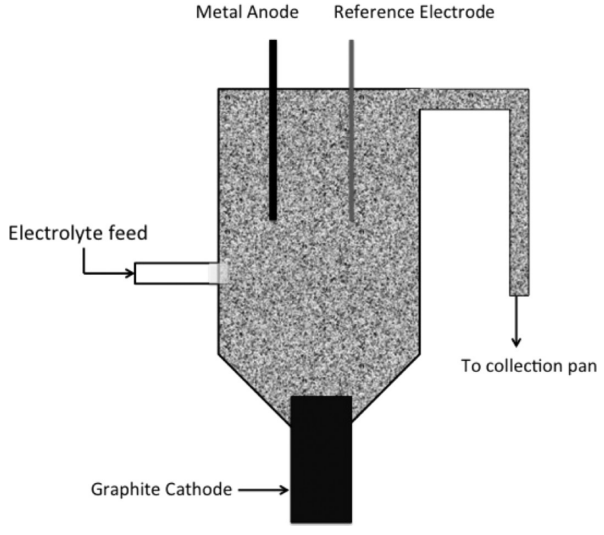

Figure 7. Schematic of the electrochemical cell for a continuous process.

■ ASSOCIATED CONTENT

Ⓢ Supporting Information

Video showing the exfoliation process, CV curves, SEM images of the expanded graphite, digital images showing the Tyndall effect and the change of the electrolyte color due to the production of graphene, TGA, histogram showing the distribution of the flakes size, and AFM, XPS, and SEM of a graphene flake dropped on a slightly oxidized copper foil. This material is available free of charge via the Internet at http://pubs.acs.org.

■ AUTHOR INFORMATION

Corresponding Authors

*E-mail: amr.abdelkader@manchester.ac.uk.
*E-mail: ian.kinloch@manchester.ac.uk.

Notes

The authors declare the following competing financial interest(s): the authors hold a patent in the area of electrochemical exfoliation.

■ ACKNOWLEDGMENTS

The authors acknowledge support from UMIP.

■ REFERENCES

(1) Novoselov, K. S.; Geim, A. K.; Morozov, S. V.; Jiang, D.; Zhang, Y.; Dubonos, S. V.; Grigorieva, I. V.; Firsov, A. A. *Science* **2004**, *306* (5696), 666−669.
(2) Castro Neto, A. H.; Guinea, F.; Peres, N. M. R.; Novoselov, K. S.; Geim, A. K. *Rev. Mod. Phys.* **2009**, *81* (1), 109−162.
(3) Geim, A. K.; Novoselov, K. S. *Nat. Mater.* **2007**, *6* (3), 183−191.
(4) Balandin, A. A.; Ghosh, S.; Bao, W. Z.; Calizo, I.; Teweldebrhan, D.; Miao, F.; Lau, C. N. *Nano Lett.* **2008**, *8* (3), 902−907.
(5) Li, X. S.; Cai, W. W.; An, J. H.; Kim, S.; Nah, J.; Yang, D. X.; Piner, R.; Velamakanni, A.; Jung, I.; Tutuc, E.; Banerjee, S. K.; Colombo, L.; Ruoff, R. S. *Science* **2009**, *324* (5932), 1312−1314.
(6) Reina, A.; Jia, X. T.; Ho, J.; Nezich, D.; Son, H. B.; Bulovic, V.; Dresselhaus, M. S.; Kong, J. *Nano Lett.* **2009**, *9* (1), 30−35.
(7) Berger, C.; Song, Z. M.; Li, T. B.; Li, X. B.; Ogbazghi, A. Y.; Feng, R.; Dai, Z. T.; Marchenkov, A. N.; Conrad, E. H.; First, P. N.; de Heer, W. A. *J. Phys. Chem. B* **2004**, *108* (52), 19912−19916.
(8) Hernandez, Y.; Nicolosi, V.; Lotya, M.; Blighe, F. M.; Sun, Z. Y.; De, S.; McGovern, I. T.; Holland, B.; Byrne, M.; Gun'ko, Y. K.; Boland, J. J.; Niraj, P.; Duesberg, G.; Krishnamurthy, S.; Goodhue, R.; Hutchison, J.; Scardaci, V.; Ferrari, A. C.; Coleman, J. N. *Nat. Nanotechnol.* **2008**, *3* (9), 563−568.
(9) Stankovich, S.; Dikin, D. A.; Piner, R. D.; Kohlhaas, K. A.; Kleinhammes, A.; Jia, Y.; Wu, Y.; Nguyen, S. T.; Ruoff, R. S. *Carbon* **2007**, *45* (7), 1558−1565.
(10) Park, S.; Ruoff, R. S. *Nat. Nanotechnol.* **2009**, *4* (4), 217−224.
(11) McAllister, M. J.; Li, J. L.; Adamson, D. H.; Schniepp, H. C.; Abdala, A. A.; Liu, J.; Herrera-Alonso, M.; Milius, D. L.; Car, R.; Prud'homme, R. K.; Aksay, I. A. *Chem. Mater.* **2007**, *19* (18), 4396−4404.
(12) Geim, A. K. *Science* **2009**, *324* (5934), 1530−1534.
(13) Ping, J. F.; Wang, Y. X.; Fan, K.; Wu, J.; Ying, Y. B. *Biosens. Bioelectron.* **2011**, *28* (1), 204−209.
(14) Lu, J.; Yang, J. X.; Wang, J. Z.; Lim, A. L.; Wang, S.; Loh, K. P. *ACS Nano* **2009**, 3 (8), 2367−2375.
(15) Wei, D.; Grande, L.; Chundi, V.; White, R.; Bower, C.; Andrew, P.; Ryhanen, T. *Chem. Commun.* **2012**, *48* (9), 1239−1241.
(16) Liu, N.; Luo, F.; Wu, H. X.; Liu, Y. H.; Zhang, C.; Chen, J. *Adv. Funct. Mater.* **2008**, *18* (10), 1518−1525.
(17) Zhong, Y. L.; Swager, T. M. *J. Am. Chem. Soc.* **2012**, *134* (43), 17896−17899.
(18) Paddon, C. A.; Compton, R. G. *J. Phys. Chem. C* **2007**, *111* (26), 9016−9018.
(19) Saito, T.; Uosaki, K. *J. Electrochem. Soc.* **2003**, *150* (4), A532−A537.
(20) Aurbach, D.; Moshkovich, M.; Cohen, Y.; Schechter, A. *Langmuir* **1999**, *15* (8), 2947−2960.
(21) Santhanam, R.; Noel, M. *J. Power Sources* **1997**, *66* (1,Äì2), 47−54.
(22) Yue, D.; Jia, Y.; Yao, Y.; Sun, J.; Jing, Y. *Electrochim. Acta* **2012**, *65* (0), 30−36.
(23) Buzzeo, M. C.; Giovanelli, D.; Lawrence, N. S.; Hardacre, C.; Seddon, K. R.; Compton, R. G. *Electroanalysis* **2004**, *16* (11), 888−896.
(24) Alheid, H.; Schwarz, M.; Stumpp, E. *Mol. Cryst. Liq. Cryst. Sci. Technol., Sect. A* **1994**, *244* (1), 191−196.
(25) Besenhard, J. O.; Theodoridou, E.; Möhwald, H.; Nickl, J. J. *Synth. Met.* **1982**, *4* (3), 211−223.
(26) Chen, Y.; Haddon, R. C.; Fang, S.; Rao, A. M.; Eklund, P. C.; Lee, W. H.; Dickey, E. C.; Grulke, E. A.; Pendergrass, J. C.; Chavan, A.; Haley, B. E.; Smalley, R. E. *J. Mater. Res.* **1998**, *13* (09), 2423−2431.
(27) Dryden, H. L.; Webber, G. M.; Burtner, R. R.; Cella, J. A. *J. Org. Chem.* **1961**, *26* (9), 3237−3245.
(28) Bergbreiter, D. E.; Killough, J. M. *J. Chem. Soc., Chem. Commun.* **1976**, *22*, 913−914.
(29) Bergbreiter, D. E.; Killough, J. M. *J. Am. Chem. Soc.* **1978**, *100* (7), 2126−2134.
(30) Ferrari, A. C.; Meyer, J. C.; Scardaci, V.; Casiraghi, C.; Lazzeri, M.; Mauri, F.; Piscanec, S.; Jiang, D.; Novoselov, K. S.; Roth, S.; Geim, A. K. *Phys. Rev. Lett.* **2006**, *97* (18), 187401.
(31) Meyer, J. C.; Geim, A. K.; Katsnelson, M. I.; Novoselov, K. S.; Obergfell, D.; Roth, S.; Girit, C.; Zettl, A. *Solid State Commun.* **2007**, *143* (1−2), 101−109.